Article Post-Print

doi:10.1016/j.jprocont.2015.05.002

Optimization-Based Assessment of Design Limitations to Air Separation Plant Agility in Demand Response Scenarios

Yanan Cao[a], Christopher L.E. Swartz[a], Michael Baldea[b,c], Stéphane Blouin[b,d]

[a] *Department of Chemical Engineering, McMaster University, 1280 Main St W, Hamilton, ON, L8S 4L7, Canada*

[b] *Advanced Control and Operations Research, Praxair Technology Center, Tonawanda, NY 14150, USA*

[c] *Present Affiliation: McKetta Department of Chemical Engineering, The University of Texas at Austin, 200 East Dean Keeton St., Stop C0400, Austin, TX 78712-0231, USA*

[d] *Present Affiliation: Defence R & D Canada - Atlantic, P. O. Box 1012, Dartmouth, NS, B2Y 3Z7, Canada*

Abstract

The significant effect that the design of a plant can have on its dynamic performance has led to methodologies for systematic analysis of the interaction between design and control, and for inclusion of dynamic performance considerations in plant design. This article focuses on the assessment of design limitations to the agility of a nitrogen plant in response to demand and electricity price fluctuations. A two-tiered approach is proposed, where a economics-based optimization problem is first solved to determine the optimal steady-state operating point, after which a dynamic optimization problem is solved to minimize a measure of the transition time to the new operating point. Design limitations to the plant's responsiveness may be inferred by analysis of the active constraints. The approach is demonstrated on a comprehensive case study based on an existing industrial nitrogen plant. The design limitations of the existing plant configuration are identified, and the potential benefits of selected design modifications to demand response operation are assessed.

Keywords: cryogenic air separation, optimization, dynamic, design, agility, demand response

1. Introduction

The impact that the design of a plant has on its dynamic performance has led to a number of research studies on the topic, particularly over the past three decades. Plants with poor dynamic performance characteristics may result in failure to meet product demand specifications, violation of operational, safety and environmental constraints, and degradation in economic performance. Optimization provides a useful and flexible framework for addressing design limitations to dynamic performance, and has been the basis for several studies, including [1, 2, 3]. Typically, an economic objective function is optimized, subject to satisfying the dynamic model equation constraints, design constraints, and path constraints on the plant input and response variables. Comprehensive reviews on approaches toward addressing this problem are provided in [4, 5, 6].

In the air separation industry, plant dynamic performance was historically judged based on the ability to reject disturbances. The agility and switchability (i.e., ability to switch between operating points quickly and optimally) were of little importance [7, 8], mainly because such plants used to experience infrequent changes in operating conditions. This is no longer the case due to electricity price deregulation in many regions, which has resulted in fluctuations in electricity price. Since electricity consumption is the major operational cost for an air separation plant, responding optimally to electricity price changes could yield significant economic benefits [9, 10]. A related effect is that customers of air separation products may also adjust their consumption level in accordance to the electricity price, thereby providing valuable demand response (DR) service and assisting the mitigation of peak loads on the electric grid [1]. These economic factors ultimately translate into frequent plant load changes that must be performed within a given (and typically short) time window. The use of steady-state simulation tools to design plants that will be subject to highly dynamic demand and utility price patterns has limitations, motivating the adoption of approaches that take the dynamics of transitions directly into account.

We review here briefly a number of studies that address the design or operation of air separation units under uncertainty. Sirdeshpande *et al.* [12] formulate a mixed-integer nonlinear programming problem (MINLP) to determine the cost-optimal configuration of an air sepa-

[1] Demand Response is defined by the Federal Energy Regulatory Commission (FERC) [11] as "Changes in electric usage by demand-side resources from their normal consumption patterns [in response to economic incentives and dynamic pricing structures] at times of high wholesale market prices or when system reliability is jeopardized."

ration unit from a number of options, given a product slate. They analyze the flexibility of the optimal design to assess the range of liquid and gaseous oxygen product for which feasible operation can be maintained. Algebraic models regressed from Aspen HYSYS simulations are used in the analysis. Zhu *et al.* [13] apply a multi-scenario approach to the design of an air separation plant to account for uncertainty in argon demand and a thermodynamic parameter. The expected cost is minimized, subject to feasible steady-state operation over all scenarios. In [14], optimal operation under demand uncertainty is considered. Steady-state process models are employed, and the formulation is extended to multiple time periods to which a parallel implementation of an interior-point optimization method is applied. Mitra and Grossmann [15] present a mixed-integer linear programming (MILP) model to determine optimal production planning under specified time-dependent demands and electricity prices. Rather than a detailed plant model, a model based on production modes, transition logic and mass balances is used.

Several studies have used dynamic models in the design and performance analysis of air separation units. White *et al.* [7] formulate a dynamic optimization problem to minimize a measure of transition time between two steady-state operating points. Approximate compartmental models are used for the distillation systems. Schenk *et al.* [16] consider integrated design and control of a cryogenic air separation plant through a mixed-integer dynamic optimization (MIDO) formulation. An economic objective function is optimized, with design variables comprising distillation column diameters and numbers of trays, control structure, and proportional-integral (PI) controller tuning parameters. Disturbances in inlet air temperature and flow rate, and liquid nitrogen feed flow rate are considered, together with a ramping specification. Miller *et al.* [8] investigate the reduction in start-up time of an air separation unit through the reintroduction of liquid collected during shutdown. The analysis is conducted through dynamic simulation studies. Nonlinear predictive control has also been investigated for air separation units, motivated largely by the need for effective control during load changes [17, 18, 19]. Xu *et al.* [19] consider in addition an upper layer supervisory control structure.

In this paper, we investigate design limitations to transitions in response to product demand and electricity price variation in an industrial nitrogen plant. We address this through a two-tiered optimization formulation, where an economically optimal steady-state operating point is first computed, followed by the solution of a dynamic optimization problem to determine an optimal trajectory to the new operating point based on minimizing a measure of transition speed. Section 2 gives a brief introduction of cryogenic nitrogen plant. The

plant model and proposed optimization formulation are described in Sections 3 and 4. A comprehensive multi-part case study is presented in Section 5, in which a number of demand and electricity price scenarios are considered and limiting constraints identified. The impact of selected design modifications on achievable transition speed is also explored. Conclusions and future research directions are presented in Section 6.

2. Process Description

Products of air separation processes play key roles in a variety of market sectors, such as petrochemical, metal, food processing and health care. The separation of air into oxygen, nitrogen and argon can be achieved by either cryogenic or noncryogenic processes [12]. The cryogenic approach for air separation is based on low-temperature distillation and is capable of producing large quantities of high purity liquid and gas phase products. On the other hand, noncryogenic processes rely on adsorption and membrane separation, and are usually economically interesting at smaller production rates. The focus of our study is on cryogenic nitrogen plants.

Fig. 1 shows a simplified schematic of major process equipment in a typical nitrogen plant. Zhu *et al.* [20] and Espie and Papageorgaki [21] provide a detailed process description. The intake air from the atmosphere is first compressed through a multi-stage compressor and then introduced to an adsorber or other purification units to remove impurities such as carbon dioxide and water. The treated air feed is cooled against the cryogenic gas product stream and waste stream from the distillation column in a multi-stream heat exchanger, typically of the plate-fin variety. A portion of the air feed is withdrawn at an intermediate point of the heat exchanger and goes through a turbine for additional cooling prior to being introduced to the column. The air feed, entering at the bottom of the column, is distilled into a high purity gaseous nitrogen stream, which leaves at the top, and an oxygen-enriched liquid which accumulates at the bottom. A portion of the overhead stream is withdrawn as the gas product while the rest is sent to the integrated reboiler/condenser to exchange heat with the oxygen-enriched stream drawn from the bottom to produce the reflux stream and the liquid nitrogen product [20, 21].

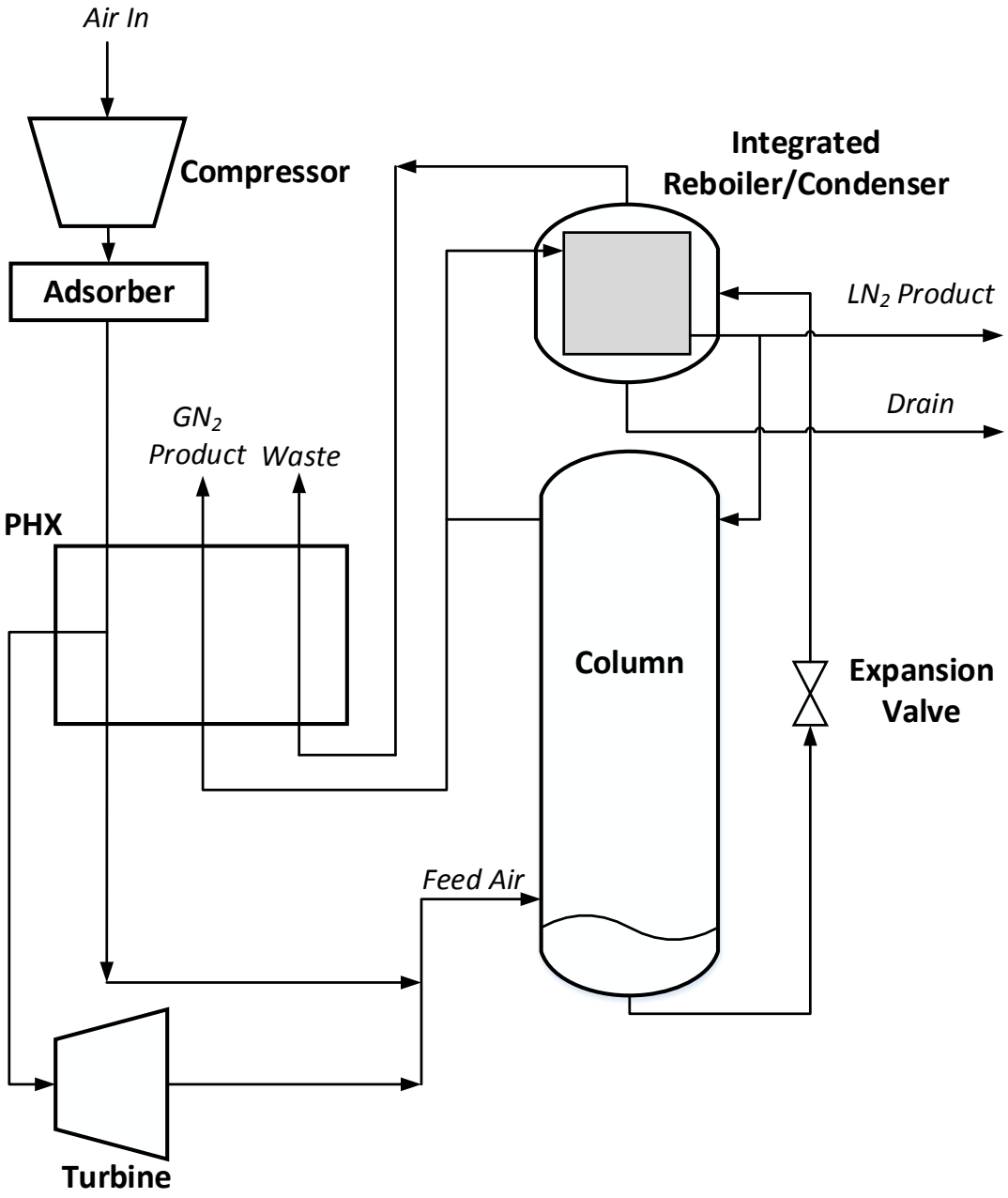

Figure 1: Nitrogen plant process diagram, as depicted in [20]. LN_2 = Liquid Nitrogen; GN_2 = Gas Nitrogen; PHX = Primary Heat Exchanger.

3. Air Separation Unit Model

In order to develop a rigorous model for the nitrogen plant, which captures the plant constraints and adequately represents its nonlinear nature, individual models were developed first and then assembled in accordance with the plant configuration. The proposed integrated plant model includes both first principles and empirical models. In our study, the following components were modeled: distillation column with integrated reboiler/condenser, primary heat exchanger, compressor, and turbine. In the remainder of this section, we briefly describe the modeling approach followed for these individual process units, and thereafter their integration into a composite dynamic model for the air separation unit (ASU) (see also [22]). Details of the model presented in this section can be found in [23].

3.1. Distillation Model

The dynamic distillation model is based on tray-by-tray component material and energy balances, following a typical approach as documented in many studies on distillation columns, such as [24, 25, 8]. Model formulations tend to differ in terms of assumptions made and specific choices of variables (such as mole fractions, total flows and liquid tray holdups versus component flows and holdups). In this work, component material and energy balances are expressed as differential equations at each column tray. Vapor-liquid phase equilibrium, thermodynamic and hydraulic models, etc., are in form of algebraic equations. These result in a general column model as an differential-algebraic equation (DAE) system. Key assumptions are:

- ternary column with components N_2, O_2 and Ar
- negligible vapor holdup, as justified in [24] for low temperature, high pressure columns
- perfect mixing and saturated liquid at each tray

Key features of our proposed model are the following:

(i) tray hydraulics are represented by the Francis Weir equation [26, 27];

(ii) vapor-liquid phase equilibrium (VLE) is captured by the Modified Raoult's Law and the Antoine equation [28];

(iii) the Margules equation for estimating activity coefficients is implemented for the consideration of non-idealities in the thermodynamics [29, 30];

(iv) Murphree tray efficiencies are used for tray non-ideality;

(v) the vapor velocity and the flooding velocity are estimated at each tray [25, 31];

(vi) the Rackett equation [32], Macleod-Sugden correlation [33, 34] and Peng-Robinson Equation of State [35, 34] are used to calculate liquid phase density, liquid surface tension and vapor phase density, respectively;

(vii) while the column is separated from the environment by a secondary container filled with insulation (known as a "cold box"), this insulation is not perfect and we introduce of a heat leakage term in the energy balance to represent heat transfer between the column and the surroundings.

The distillation model in its basic form under the above assumptions results in a high-index DAE system, due mainly to the assumption of negligible vapor holdup as the vapor flows cannot be solved directly from the algebraic equations [36]. High-index DAE systems tend to be very sensitive to input changes and more difficult to initialize and integrate over time [37, 38]. Reformulations have been proposed to reduce the index of distillation models [18, 36, 39]. The main idea is to derive a mathematically equivalent algebraic expression for the time derivative term of the energy balances. The manual index reduction approach implemented in our study is similar to those used in [18, 39].

The integrated reboiler and condenser (IRC), as shown in Fig. 1, includes two sub-models: one for the condenser side and the other for the reboiler side. It was assumed that there is no heat loss between the reboiler and the condenser. For the condenser model, it was assumed that the condenser side has neither material nor energy holdups [20]. The vapor drawn into the condenser would go through a phase change and leave the condenser as a saturated liquid. It was further assumed that conditions in the condenser are the same as the top tray vapor (i.e., temperature, pressure and compositions). The reboiler is modeled in a similar way as the column tray except that a steady-state energy balance is used, with the energy balance expression derived in a similar manner as in [24]. It was assumed that the reboiler side pressure is assigned. The flow rate of the bottom liquid and the drain are controlled using two proportional-integral level controllers.

3.2. Primary Heat Exchanger Model

The primary heat exchanger (PHX) in the industrial plant considered in this study is a plate-fin heat exchanger consisting of stacked layers of fins with parting sheets used to

separate different layers. The three process streams are distributed into different layers in an alternating pattern. The system was modeled as three streams in contact with each other, and partitioned axially into segments, similar to the approach followed by Miller *et al.* [8] for the two streams considered in their system. As with any such discretization, the number of segments chosen has to be large enough to avoid the occurrence of temperature crossover. The configuration and dimensions of the industrial PHX were used to calculate the volumes occupied by the three streams, and also to estimate the volume of metal from which the mass of metal could be computed from the known metal density.

Changes in metal wall temperature as well as the process stream temperatures with respect to time are captured using segment-wise dynamic energy balances. Thermal properties of the streams required in the energy balances, including molar density and enthalpy, are computed using algebraic equations. Corresponding to the location of the air withdrawal (Fig. 1), the PHX is divided into two zones: one before the air removal (zone 1), and one after the air removal (zone 2). It was assumed that there is no phase change in zone 1, but a phase change occurs in the air stream in zone 2 with the air leaving the PHX as a saturated liquid. Pressure drop of the processing streams across the heat exchanger is considered, with a constant pressure drop across each segment assumed.

3.3. Compressor and Turbine Models

The compressor and turbine are modeled as systems of algebraic equations due to their fast dynamics. The multi-stage compressor was modeled using available compressor maps, coupled with use of polytropic efficiency relationships. The given compressor map provides correlations of discharge pressure with stream volumetric flow rate and inlet guide vane opening. Compressor surge lines were also extracted from the compressor map. Power consumption and discharge temperature of the compressor were estimated following the theoretical approach as explained in Brown [40]. The turbine model was developed in a similar manner, but in this case, instead of turbine maps, correlations derived from historical data for turbine speed, discharge pressure and stream flow rate were used.

3.4. Plant Model

The individual models were assembled in accordance with the plant configuration, and coded using the commercial software package `gPROMS` [41], which was used for all simulation and

optimization calculations in this work. A parameter estimation step was conducted to reconcile the model with available plant data using the steady-state version of the composite plant model. Plant data used were the gas nitrogen product (GN_2) production rate, product purity, compressor feed rate, reboiler temperature, outlet PHX temperature of the GN_2 stream, column liquid and vapor feed temperatures, and turbine discharge pressure and temperature. Model parameters estimated were the tray efficiency (assumed uniform), IRC drain and column sump flow rates, base PHX UA values, and the turbine polytropic exponent. Other required model parameters such as equipment sizes were specified according to available plant information or estimates from industrial personnel. `gPROMS` was used to perform the parameter estimation task. The objective function for the `gPROMS` parameter estimation in this case is of the maximum-likelihood type [42]:

$$\Phi_{PE} = \frac{N_m}{2}\ln(2\pi) + \frac{1}{2}\min_{\boldsymbol{\theta}}\left\{\sum_{i=1}^{NV}\sum_{j=1}^{NM_i}\left[\ln\left(\sigma_{ij}^2\right) + \frac{(\widetilde{z}_{ij} - z_{ij})^2}{\sigma_{ij}^2}\right]\right\} \tag{1}$$

where N_m and NV are the total number of measurements used and measured variables, respectively; NM_i is the number of available measurements of variable i; σ_{ij}^2 is the variance of the j^{th} measurement of variable i; $\widetilde{z}_{ij}$ and z_{ij} denote j^{th} measured value and predicted value of variable i; and θ represents the model parameters to be estimated. After model validation, the maximum absolute relative error between the model prediction and the corresponding measurements was determined to be less than 2 %.

4. Optimization Formulation

The primary purpose of this study is to identify factors that limit the dynamic performance of the plant during transition in response to dynamic market conditions. The underlying assumption is that except during transitions, the plant operates at a steady-state operating point. Thus, we ensure that under normal conditions, the steady-state operating point is economically optimal.

The optimization methodology adopted follows a two-tiered approach. The first tier solves a steady-state optimization problem to determine the economically optimal operating point corresponding to new market conditions (i.e., customer demand requirements or electricity price in this study). The second tier is to obtain a set of trajectories of the manipulated variables to achieve a fast transition to the pre-determined operating point, determined as the solution to a dynamic optimization problem. While simply applying step changes to the

manipulated inputs to their new steady-state values may seem attractive, this could result in constraint violations in the system response during the transition, which we demonstrate later. We note that by considering changes in the manipulated variables directly, the best possible plant performance obtained is independent of the plant control system, and thus serves as a control performance benchmark.

In the next subsections we present the detailed optimization formulations for the two tiers.

4.1. Tier 1: Economic Steady-state Optimization

We remark first that the product demand must be satisfied, and can be done by evaporation of pre-stored liquid N_2 if the amount gas nitrogen (GN_2) produced by the plant is insufficient. By solving the first tier optimization problem, an economically optimal steady-state operation point is obtained (i.e., the desired GN_2 production rate, as well as the optimal control input values), which is then provided to the dynamic optimization formulation.

4.1.1. General Form

The steady-state optimization framework takes the following form:

$$\max_{\mathbf{u}, F_{evap}} \Phi_{ss} = C_{\mathrm{GN}_2}\left(F_{\mathrm{GN}_2,prod} + F_{evap}\right) - C_{elec}W_{poly} - C_{evap}F_{evap} \tag{2a}$$

$$\text{subject to:} \quad \mathbf{f}(\dot{\mathbf{x}} = \mathbf{0}, \mathbf{x}, \mathbf{z}, \mathbf{u}, \mathbf{p}) = \mathbf{0} \tag{2b}$$

$$\mathbf{g}(\mathbf{x}, \mathbf{z}, \mathbf{u}, \mathbf{p}) = \mathbf{0} \tag{2c}$$

$$\mathbf{h}(\mathbf{x}, \mathbf{z}, \mathbf{u}, \mathbf{p}) \leq \mathbf{0} \tag{2d}$$

where $\mathbf{x}$, $\mathbf{z}$, $\mathbf{u}$ and $\mathbf{p}$ are differential state, algebraic state, control input and parameter vectors, respectively. Parameters and variables in the objective function are: sales price of gas nitrogen (C_{GN_2}), compressor and evaporation costs (C_{elec} and C_{evap}), production rate of gas nitrogen ($F_{\mathrm{GN}_2,prod}$), rate of evaporation of pre-stored liquid N_2 (F_{evap}) and compressor power consumption (W_{poly}). $\mathbf{f}$ and $\mathbf{g}$ comprise the DAE plant model equations and $\mathbf{h}$ includes variable bounds (i.e., for $\mathbf{x}$, $\mathbf{z}$, $\mathbf{u}$), operational constraints, product specification constraints and constraints required in the model. The components of $\mathbf{u}$ comprise

- standard volumetric flow rate of air feed to the compressor ($\dot{V}_{std}$)
- molar flow rate of liquid air feed to the column from the PHX ($F_{liq\ air}$)

- LN_2 production rate (F_{LN_2})
- gas draw fraction ($r_{gas\ draw}$): defined as the fraction of the column top vapor being sent to the PHX, i.e., GN_2 produced ($r_{gas\ draw} = F_{GN_2,prod}/V_{top}$)

The evaporation rate of LN_2 for unmet demand (F_{evap}) is a decision variable used only in the steady-state optimization tier. It is introduced to the GN_2 product stream after the PHX and assumed to be available from another facility or can be drawn from a storage tank.

4.1.2. Constraints

Constraints considered in this tier include operational constraints, production requirements and constraints for ensuring physical consistency in model predictions, as described below.

Operational constraints

The operational constraints comprise surge constraints at the compressor and the flooding constraints at all column trays. To prevent surging, the compressor should operate away from the surge line with a safety margin of ε_{surge} ($\varepsilon_{surge} \geq 0$)

$$\dot{V}_{std} - \dot{V}_{critical} \geq \varepsilon_{surge} \tag{3}$$

where $\dot{V}_{critical}$ is the volumetric flow rate corresponding to surge conditions as given by the compressor map. At any column tray n, the fractional flooding ($\alpha_n^{flooding}$, the ratio of the gas velocity to the corresponding flooding velocity) should not exceed 1. With a non-negative tolerance, $\varepsilon_{flooding}$, this gives

$$1 - \alpha_n^{flooding} \geq \varepsilon_{flooding} \tag{4}$$

Production Specification Constraints

Regardless the market conditions, the plant is obligated to supply qualified product within a specified steady-state maximum impurity limit ($Impurity_{ss}$)

$$Impurity - Impurity_{ss} \leq 0 \tag{5}$$

to meet certain customer demand D, either by GN_2 production or LN_2 evaporation without any offsets as demand satisfaction is strictly required

$$(F_{GN_2,prod} + F_{evap}) - D \geq 0 \tag{6}$$

We do not consider in this study production that exceeds demand with possible local storage of excess liquefied product. This would require a larger time horizon to capture the potential economic benefit of such a strategy. Thus, we limit the production by the demand within a tolerance, ε_{op} ($\varepsilon_{op} \geq 0$):

$$(F_{\mathrm{GN}_2,prod} + F_{evap}) - D \leq \varepsilon_{op} \tag{7}$$

Modeling Constraints

The constraints discussed previously are required by the actual process. However, there are other constraints that are enforced to ensure that the model predictions are physically consistent. The primary heat exchanger model design and operation are such that a phase change occurs in the air stream downstream of the turbine air withdrawal. This means that the air feed from zone 2 should be in the liquid phase with outlet pressure, $P_{out,air}$, greater than its bubble point pressure with a safety margin ε_{bbl} ($\varepsilon_{bbl} > 0$) [28]:

$$P_{out,air} \geq \sum_{i=1}^{NC} y_{air,i} P_{out,i}^{sat} + \varepsilon_{bbl} \tag{8}$$

On the other hand, the turbine air should be in the vapor phase with the stream pressure, $P_{wd,air}$, less than the corresponding dew point pressure with a safety margin ε_{dew} ($\varepsilon_{dew} > 0$):

$$P_{wd,air} + \varepsilon_{dew} \leq 1 / \left[\sum_{i=1}^{NC} y_{air,i} / P_{wd,i}^{sat} \right] \tag{9}$$

$P_{out,i}^{sat}$ and $P_{wd,i}^{sat}$ are evaluated using the Antoine equation at the outlet and withdrawal point temperatures. In the IRC model, to ensure the correct direction of heat transfer, the temperature difference between the reboiler and the condenser is required to satisfy

$$T_{cond} - T_{reb} > 0. \tag{10}$$

4.2. Tier 2: Dynamic Optimization

The second tier of the optimization is to transition the plant optimally from the initial operating point to the new operating point determined in Tier 1. It would be desirable for the plant to move to a new production load as rapidly as possible without violating any constraints.

4.2.1. General Form

Direct minimization of the transition time was found to result in numerical difficulties, thus an objective function that combines transition time with a trajectory-tracking component was used. This bears some similarity to formulation in [7] where a trajectory tracking objective function was used as an indirect measure of response speed. The optimization problem is posed in the following manner:

$$\min_{\mathbf{u}(t),t_f} \Phi = t_f \left\{ \int_{t_0}^{t_f} \left[1 - \frac{F_{\mathrm{GN}_2,prod}(t)}{F^*_{\mathrm{GN}_2,prod}} \right]^2 dt + \sum_{i=1}^{N_u} w_i \left[1 - \frac{u_i(t_f)}{u_i^*} \right]^2 \right\} \tag{11a}$$

$$\text{subject to:} \quad \mathbf{f}(\dot{\mathbf{x}}(t), \mathbf{x}(t), \mathbf{z}(t), \mathbf{u}(t), \mathbf{p}, t) = \mathbf{0} \tag{11b}$$

$$\mathbf{g}(\mathbf{x}(t), \mathbf{z}(t), \mathbf{u}(t), \mathbf{p}, t) = \mathbf{0} \tag{11c}$$

$$\mathbf{h}(\mathbf{x}(t), \mathbf{z}(t), \mathbf{u}(t), \mathbf{p}, t) \leq \mathbf{0} \tag{11d}$$

$$\mathbf{h}_f(\mathbf{x}(t_f), \mathbf{z}(t_f), \mathbf{u}(t_f), \mathbf{p}, t_f) \leq \mathbf{0} \tag{11e}$$

$$\dot{\mathbf{x}}(t_0) = \mathbf{0} \tag{11f}$$

$$t_0 \leq t \leq t_f \tag{11g}$$

In the above, $F^*_{\mathrm{GN}_2,prod}$ and u_i^* represent the optimal values of the gas nitrogen product rate and input variables as determined in Tier 1, N_u is the number of control inputs, and the w_i are penalty parameters. $\mathbf{h}_f$ represents a set of terminal constraints. We remark that the second term in Eq. (11a) essentially vanishes at the optimal solution due to the end-point constraints on the control inputs; however, its presence aids the progress of the optimization.

4.2.2. Constraints

In this tier, the optimal solution has to not only satisfy those constraints from the steady-state optimization stage, but also some additional constraints that regulate the system behavior during the transition.

Path Constraints

Except for the demand satisfaction constraint, all constraints considered in Tier 1 are translated into path constraints. In this work, path constraints are transformed into combinations

of interior-point constraints and end-point inequality constraints, which corresponds to the hybrid approach to handling path constraints proposed in [43]. Dummy variables are used to track the accumulated squared constraint violations over the time horizon. To illustrate, the product impurity constraint,

$$Impurity(t) \leq Impurity_{path} \tag{12}$$

is formulated as the end-point inequality constraint:

$$\epsilon_{impurity}(t_f) \leq \varepsilon_{impurity} \tag{13}$$

with $\epsilon_{impurity}$ defined as:

$$\frac{d\epsilon_{impurity}(t)}{dt} = \left[\max\left(0,\ Impurity(t) - Impurity_{path}\right)\right]^2 \tag{14}$$

and the interior-point constraints

$$Impurity(\bar{t}_j) \leq Impurity_{path}, \quad j = 1, ..., N_J \tag{15}$$

where $\varepsilon_{impurity}$ is a pre-determined threshold and $\bar{t}_j$ is the time corresponding to the jth interior point. Eqs. (13) and (14) correspond to

$$\int_{t_0}^{t_f} \left[\max\left(0,\ Impurity(t) - Impurity_{path}\right)\right]^2 dt \leq \varepsilon_{impurity} \tag{16}$$

Also, as the value of maximum allowable impurity level during transition may be different from that for the steady-state case, the impurity level at the new operating point is also required to satisfy the steady-state operation requirements:

$$Impurity(t_f) \leq Impurity_{ss} \tag{17}$$

Additional path constraints are applied to the liquid levels in the reboiler and sump to prevent overflow or emptying:

$$l_{LB} \leq l(t) \leq l_{UB} \tag{18}$$

Model Simulation Constraints

Similar to [7], we also require that when the plant completes the transition, it has to be at steady-state. This is achieved by imposing two additional constraints: one on the manipulated variables

$$\mathbf{u}\left(\bar{t}_{N_J-1}\right) = \mathbf{u}\left(\bar{t}_{N_J}\right) \tag{19}$$

and the other on the differential state variables

$$\sum_{i=1}^{N_{\mathbf{x}}} \left[\frac{dx_i(t_f)}{dt}\right]^2 \leq \varepsilon_{ss} \tag{20}$$

where ε_{ss} is a sufficiently small tolerance, N_J is the number of control intervals, and $N_{\mathbf{x}}$ is the number of differential variables. Theoretically, when reaching the new steady-state, Eq. (20) should have a value of zero, but due to computational roundoff errors, enforcing this requirement may result in optimization difficulties. Moreover, one only needs to enforce this constraint on the slowest variable. The selection of the slowest variable can be made based on dynamic simulation results.

To force the system to reach the pre-determined economically optimal operating point, we require the control inputs and desired production rate to reach a neighborhood of the desired values at the end of the time horizon,

$$-\varepsilon_i \leq 1 - \frac{u_i(t_f)}{u_i^*} \leq \varepsilon_i, \quad -\varepsilon_{prod} \leq 1 - \frac{F_{\mathrm{GN}_2,prod}(t_f)}{F^*_{\mathrm{GN}_2,prod}} \leq \varepsilon_{prod} \tag{21}$$

where ε_i and ε_{prod} are specified tolerances and the $*$ marks desired values.

4.2.3. Handling Optimization Decision Variables

This section explains how the decision variables are handled in the optimization problem in the second tier.

Valve Dynamics

In reality, the actual value of a manipulated variable requires some time to reach its set-point due to delay and valve dynamics. To approximately capture this phenomenon, we introduce a set of dynamic equations

$$\tau_i \frac{du_i}{dt} = u_i^{sp} - u_i, \quad i = 1, ..., N_u \tag{22}$$

where τ_i is the response time constant and the superscript *sp* indicates a set point. In addition, this also helps to smooth the input trajectory, hence reduces computation difficulties [44]. In this work, values of τ_i are set to be very small (i.e., a few seconds).

Control Vector Parametrization

The optimal control inputs are determined using control vector parametrization. In this study, the time horizon of interest is divided into N_J control intervals, and the continuous control action approximated using piece-wise linear profiles with continuity at interval boundaries. This adds some additional differential equations to the system. Using set-points of the control inputs, we have:

$$\frac{du_i^{sp}}{dt} = a_{i,j}, \quad t \in [\bar{t}_j, \bar{t}_j + \delta_j],\ i = 1, ..., N_u, j = 1, ..., N_J \tag{23}$$

where $a_{i,j}$ is the slope of the control trajectory of input i in control interval j, $\bar{t}_j$ and δ_j are starting time and duration time of control interval j. This also requires additional initial conditions. At the initial steady-state, control inputs should be at their set-points

$$u_i^{sp}(0) = u_{i,0}, \quad i = 1, ..., N_u \tag{24}$$

The initial steady-state also implies that there is no change in the control trajectory (i.e., slopes in this case)

$$a_{i,0} = 0, \quad i = 1, ..., N_u \tag{25}$$

The optimization variables are the set of parameters that define the control trajectory. In this case, it would be the slope set, namely

$$a_{i,j}, \quad i = 1, .., N_u; j = 1, .., N_J$$

The duration time of each control interval can be specified or optimized.

After applying these techniques, the true form of the objective function for the second tier becomes:

$$\min_{\mathbf{a},\boldsymbol{\delta}} \Phi = t_f \left\{ \int_{t_0}^{t_f} \left[1 - \frac{F_{\mathrm{GN}_2,prod}(t)}{F^*_{\mathrm{GN}_2,prod}} \right]^2 dt + \sum_{i=1}^{N_u} w_i \left[1 - \frac{u_i(t_f)}{u_i^*} \right]^2 \right\} \tag{26}$$

where $\mathbf{a}$ and $\boldsymbol{\delta}$ are vectors of control profile coefficients and control interval durations, respectively.

5. Case Study

5.1. Steady-state Optimization

As explained in the formulation section, the steady state optimization is intended to obtain the desired operation points under the new scenarios. The decision variables selected in this

study are as defined in Section 4.1.1. Scenarios considered in this study include: (1) demand fluctuations (i.e., positive and negative changes in demand requirements covering the range from +30 % to −30 %), and (2) electricity price increases (i.e., 2 and 4 times the base case value) with and without the demand satisfaction requirement. Details of each scenario and corresponding steady-state optimization results are presented in Table 1. Absolute and relative tolerances of the optimizer are set to 10^{-5}. The parameter ε_{surge} in Eq. (3) is assigned to be 0, and ε_{op} in Eq. (7) is assigned to be 0.005 % of $F_{prod,base}$. Safety margins of 0.01 are used in modeling constraints (8) and (9).

If the value of the constrained variable is within $\pm\ 10^{-4}$ from the corresponding bound value, it is marked as an active constraint in Table 1. Data in the table are reported as ratios to reference values. The evaporation rate is reported as percentage of the base case optimal (i.e., 0 % demand change) GN_2 production rate; the rest of the variables in Table 1 are presented as ratios to their corresponding base case values. The results presented are not guaranteed to be globally optimal due to the nonconvexity of the problem. However, while solving the problem, a number of different initial guesses were provided in each case, and the best solution is reported. The results of the case studies are discussed in the following sections.

5.1.1. Demand Fluctuation

The cases corresponding to demand changes were solved with all the constraints described in Section 4.1. As shown in Table 1, in the optimized cases, the LN_2 production is at its lower bound as there is no revenue associated with it. Note that the value 1 of LN_2 production in Table 1 corresponds to its lower bound. Also, the optimization results indicate that it is optimal to utilize available plant capacity before evaporating pre-stored LN_2 to meet the demand (i.e., evaporation only occurs with 20 % and 30 % demand increases, where the plant production is limited by the column flooding constraint). This is due to the high evaporation cost relative to the price of the GN_2 product. In all optimized cases, except for the -30 % and -20 % demand change scenarios, the plant operates at its maximum allowable steady state impurity level defined in Eq. (5) (i.e., indicated by the symbol "X" in Table 1). By doing so, more GN_2 product can be generated from the same amount of air feed. This can be seen from nitrogen recovery values in Table 1. Recall that the recovery of 1 corresponds to the base case value. In cases of -30 % and -20 % demand changes, it would be optimal in the absence of constraints for the plant to operate at the maximum allowable impurity level. However, it is impossible to reduce the feed flow rate to the value corresponding to the maximum

Table 1: Steady-state optimization results for changing demand and electricity price.[a]

		Demand							Electricity Price		
		0%	-30%	-20%	-10%	10%	20%	30%	$2P_{elec}$	$4P_{elec}$	$4P_{elec} + D$ [b]
Decision Variables	LN_2 Production	1.00	1.00	1.00	1.00	1.00	1.00	1.00	1.00	1.00	1.00
	Gas Draw Fraction to PHX	1.00	0.79	0.90	1.00	1.00	1.01	1.01	1.01	1.00	1.00
	Air Feed	1.00	0.89	0.89	0.90	1.10	1.13	1.13	1.13	0.89	1.00
	Liquid Air	1.00	1.28	1.22	1.16	0.86	0.47	0.47	0.47	1.17	1.06
	Evaporation Rate	0	0	0	0	0	6.28	16.28	0	0	0
Objective Function		1.00	0.56	0.73	0.88	1.12	0.95	0.61	0.41	-0.97	-1.01
Tracking Variables	Power	1.00	0.90	0.90	0.92	1.06	1.10	1.10	1.10	0.91	0.99
	Nitrogen Recovery[c]	1.00	0.79	0.90	0.99	1.00	1.01	1.01	1.01	1.00	1.00
	GN_2 Production	1.00	0.70	0.80	0.90	1.10	1.13	1.13	1.13	0.89	1.00
Active Constraints[d]	Maximum Allowable Impurity	X			X	X	X	X	X	X	X
	Surge Constraint		X	X						X	
	Bubble Point Constraint at PHX	X	X	X	X					X	X
	Dew Point Constraint at PHX						X	X	X		
	No Overproduction	X	X	X	X	X			N/A	N/A	
	Demand Satisfaction						X	X	N/A	N/A	X
	Flooding						X	X	X		

[a] Data in the table are scaled values. Except for evaporation rate, which is reported as % of the base case air feed flow rate, the others are represented as ratios to their corresponding values at the base case (i.e., optimized 0 % demand change).

[b] Solved with demand satisfaction requirement. The required demand is the base case production rate.

[c] N_2 recovery rate in GN_2 and LN_2 products, defined as ratio of N_2 in product streams to N_2 in the air feed to the system.

[d] The symbol "X" denotes that a particular constraint is active at the solution point.

allowable impurity as it is below the surge flow rate of the compressor. This is indicated by the active surge constraint of the compressor in these cases. Without overproduction, the plant operates with a lower recovery ratio and purer GN_2 product as more top tray vapor returns to the column as reflux rather than GN_2 product. The optimization results agree with expectation. For cases having large demand increases (i.e., +20 % and +30 %), the flooding constraint limits the plant performance. These active constraints imply that the operating window of the plant is defined by the flooding constraint (i.e., upper bound) and the surge constraint (i.e., lower bound) with respect to feed flow rate.

5.1.2. Electricity Price Change

For the electricity price change cases, without the demand satisfaction requirement, the total GN_2 supply (i.e., production plus evaporation) is not required to meet a particular demand, but should not drop below 70 % of the specified base case production rate (i.e., cases "$2P_{elec}$" and "$4P_{elec}$" in Table 1). The end-point inequality constraints on GN_2 production (Eqs. (6), (7)) are now replaced by

$$(F_{\mathrm{GN}_2,prod} + F_{evap}) - 0.7F_{prod,base} \geq 0.$$

When demand satisfaction is required (i.e., case "$4P_{elec} + D$"in Table 1), Eq. (6) is imposed. Other setups are the same as described in the demand change cases.

The general trends observed in the electricity price scenarios are consistent with those in the demand fluctuation cases. As there is no constraint that eliminates overproduction in electricity price change scenarios, the plant is able to maximize the amount of top tray vapor drawn as GN_2 product, regardless of the actual demand requirement. In the "$4P_{elec}$" case, it is optimal to run at a reduced feed rate; however, the optimal policy is to maximize N_2 recovery by operating at the maximum allowable impurity level. As with the 20 % and 30 % demand decrease cases, the surge constraint of the compressor becomes active when the feed flow rate reduces in the "$4P_{elec}$" case. Optimization results of the 2 times electricity price case agree with those of the +20 % and +30 % demand cases (i.e., operating at maximum allowable impurity and active flooding constraint). As GN_2 supply is not forced to meet a particular demand, LN_2 evaporation rates are kept at zero in the "$2P_{elec}$" and "$4P_{elec}$" cases. When demand satisfaction is required (i.e., case "$4P_{elec} + D$" in Table 1), it is still optimal to utilize the plant capacity to meet the demand instead of evaporating pre-stored LN_2. This is expected due to the high evaporation cost used in the case study (which reflects the operating expenses required to generate the stored liquid nitrogen).

Optimization results of the electricity price cases show an interesting insight on the break-point between revenue from production and cost due to electricity consumption. When the electricity price increases, before it reaches a critical value, it is optimal to operate at the maximum plant capacity (defined by the flooding constraint). Within this range, the compression cost is still lower than the sale price of the GN_2 product. However, once the electricity price exceeds a break-point, it is beneficial to reduce production, or even shut the plant down if possible, since the plant loses money by continuing production. Detailed analyses with plant shutdowns are beyond the scope of this work, as it requires hybrid models containing the shutdown mode. Table 1 indicates that for the price information used in this study, the break point is between the 2 times and 4 times electricity price.

5.1.3. Grid Load Shedding

Air separation units are significant electricity consumers and have significant potential to provide demand response (DR) service to the power grid via load reduction (also known as "load shedding" [45, 46]) service, i.e., a deliberate reduction in production rate during periods of peak grid demand (which are, in turn, reflected in peak energy prices). As illustrated above, during such periods, customer requirements for air separation products can be satisfied by evaporating stored liquid, generated at off-peak times. A recent study [9] suggested that operating ASUs in this manner can improve profitability, and motivated further work on optimal scheduling of ASU operations, along with appropriate capacity planning for DR scenarios [47, 48].

Fig. 2 illustrates the demand response potential of the plant under consideration, showing that a reduction of 10% of the nominal grid load (in terms of compression power) is possible, conceivably with no service disruption to the nitrogen customer.

Our results in the next subsection emphasize the importance of process *dynamics* and the speed of response of a process when considering its operation as a DR actor in the grid. We also emphasize that the integration of production scheduling and control is crucial to fully realize the economic and grid-balancing benefits that can be derived from DR operation [49]; namely, the decisions related to the timing and duration of increased production and load shedding must be coordinated in a manner that ensures that the former generates sufficient liquid product to support the latter, in the most economically advantageous fashion.

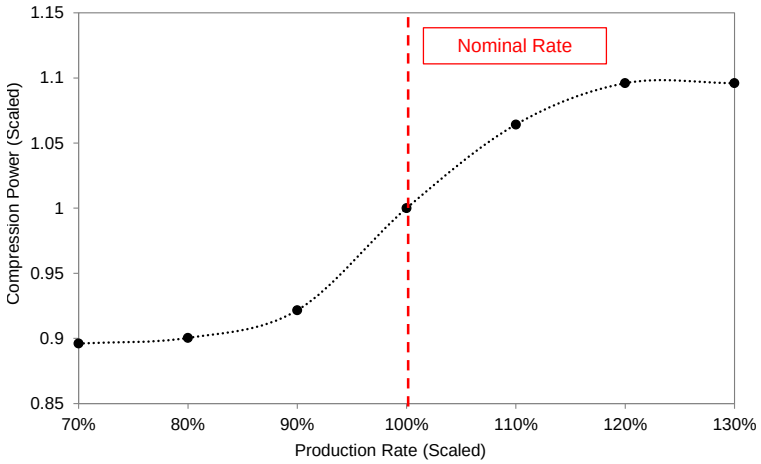

Figure 2: Grid load shedding potential of the plant as a function of production capacity.

5.2. Dynamic Optimization for Existing Design

Case studies in this section consider transition to the optimized steady-state operating point without design modifications by using the first four control inputs defined in Section 5.1. Dynamic optimizations were preformed for ± 20 % and ± 10 % demand change cases. In this paper, we will present results for the ± 20 % cases. General trends for the ± 10 % cases are similar to the ± 20 % scenarios. The objective function used is Eq. (26).

The total time horizon was divided into 3 periods as shown in Table 2. The initial period is to ensure that transitions start at the initial steady-state operating point. At the end of the initial period, demand changes occur. In the control period, the plant takes action to respond to the market changes. Both the control trajectory slopes and control interval duration time are optimized. The final settling period is to ensure that the system settles at a new steady-state and is stable after a period of time. The maximum impurity level during transitions is set to twice the limit imposed at steady-state.

5.2.1. Positive 20 % Demand Change

Before applying dynamic optimization, a step test was performed to change the plant operation from the optimal base case to the optimized steady-state corresponding to a 20 % demand increase. Fig. 3 plots the largest vapor velocity to flooding velocity ratio within the column. As shown, a direct step change is not desirable/applicable as it violates the flooding constraint during the transition. This provides an incentive for performing dynamic optimization.

Table 2: Dynamic Optimization Setup

Period	Intervals	Duration Time	Input Slopes[a]
Initial [b]	1	Assigned (1 hr)	Assigned to 0
Control	N_J	Optimized $\left(\sum_{j=1}^{N_J} \delta_j\right)$	Optimized
Settling [c]	1	Assigned (3 hr)	Assigned to 0

[a] $a_{i,j}$ in Eq. (23).

[b] To ensure that the transition starts at the initial steady-state.

[c] To ensure that the system settles at a new steady-state.

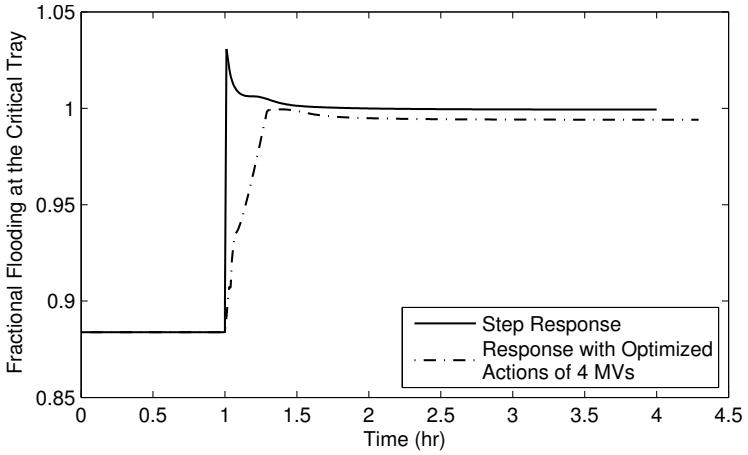

Figure 3: Fraction of vapor velocity to flooding velocity at critical tray for 20 % demand increase case

Fig. 4 presents dynamic responses of the GN_2 production and product impurity as well as the optimized control actions of selected manipulated variables. The variables are scaled in the same manner as in Table 1. The trajectory of resulting GN_2 production is close to a step with small offsets at the beginning. There is an initial peak in product impurity, which is due to a temporary decrease of internal liquid to vapor ratio. With an increase in the air feed into system, the amount of vapor air feed into the column increases, especially when the liquid air to the column is reduced. This leads to an immediate increase in the column internal vapor flow. Meanwhile, the internal liquid flow requires time to catch up with such change due to the column dynamics. In addition, optimal trajectories of LN_2 production and gas draw fraction to the PHX (not shown here) increase sharply before decreasing again, which cause even less liquid to return to the column as reflux compared to the vapor flow. However, this change in the internal liquid to vapor ratio diminishes after the system settles at the desired steady-state, with all manipulated variables reaching their desired values within allowable tolerances. In contrast to the result for the direct step change, with the optimized control actions the flooding constraint is active but not violated anymore (see Fig. 3). The dew point constraint at the PHX is another active constraint determined from the `gPROMS` solution. These active constraints illustrate that in order to increase capacity or obtain improved transient performance, tray re-design and PHX re-sizing should be considered.

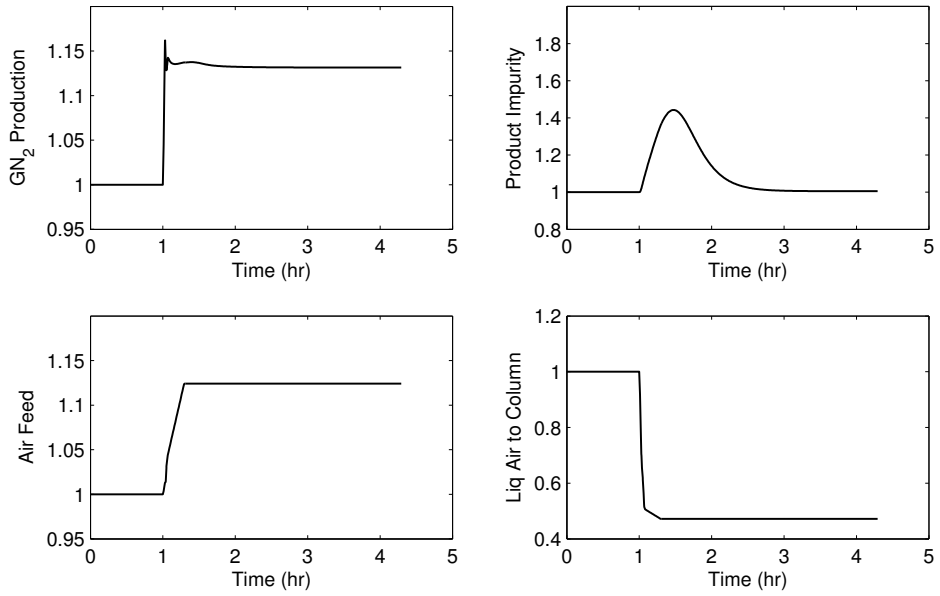

Figure 4: Responses of the scaled variables for the 20 % demand increase case with optimized control actions.

5.2.2. Negative 20 % Demand Change

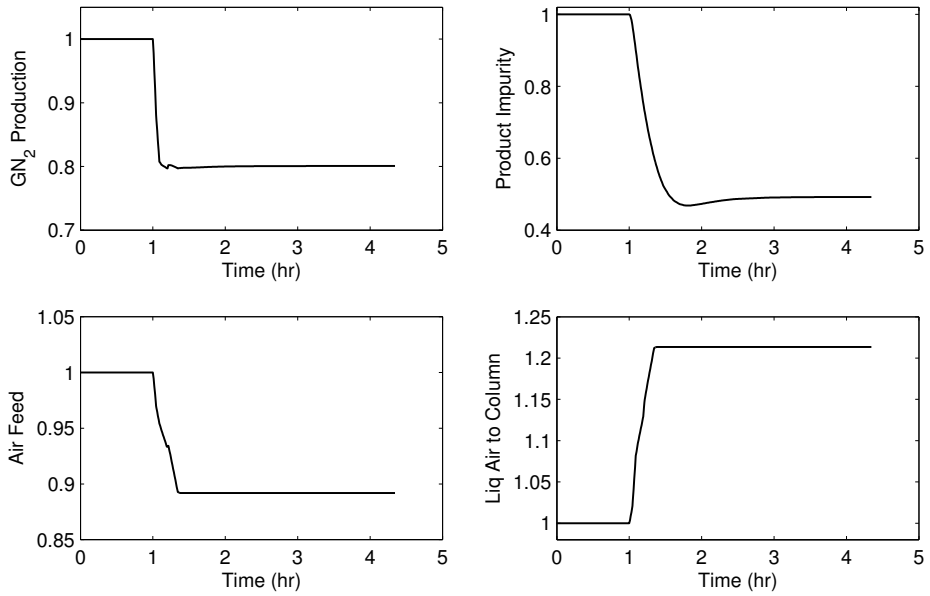

Figure 5: Responses of the scaled variables for the 20 % demand decrease case with optimized control actions.

Fig. 5 shows the optimal dynamic responses of the GN_2 production, product impurity, and control actions of selected manipulated variables for a 20 % decrease in GN_2 product demand. The product impurity in this case decreases first then increases to the new steady-state value. However, as the impurity level at the new operating point is low, the trough is not that noticeable. Again, the system reaches a stable operating point with all control inputs at their optimal values and negligible offsets in GN_2 production. The response of the GN_2 production is step like. The surge constraint of the compressor and the bubble point constraint at the PHX are active during the transition, suggesting compressor and PHX re-sizing/re-design to improve performance for plant turndown.

5.3. Effects of Design Modifications

We note that altering column, heat exchanger and compressor configurations are capital intensive and require major plant retrofits. In this section we investigate some more cost-effective modifications for reshaping the dynamic performance of the plant under consideration.

5.3.1. Introducing External Liquid Nitrogen during Transitions

Introducing external LN_2 back to the column during transitions is one of the design modifications we proposed, particularly for cases where the flooding constraint may be active during transitions. Miller *et al.* [8] demonstrated that re-introducing external liquid to the column can reduce start-up times. As the flooding constraint limits the plant performance during transitions for demand increase cases, it might be beneficial to introduce pre-stored LN_2 back to the column during transitions without altering the tray design. For simplicity, we assumed that the pre-stored LN_2 is at the same conditions and hence has the same properties as the reflux to the column. Control profiles of the external liquid nitrogen flows are treated in the same way as other system inputs as described in Section 4. The general form of the objective function used for evaluating this design modification used in this paper is:

$$\min_{\mathbf{a},\mathbf{b},\delta} \Phi = t_f \left\{ \int_{t_0}^{t_f} \left[1 - \frac{F_{\mathrm{GN}_2,prod}(t)}{F^*_{\mathrm{GN}_2,prod}} \right]^2 dt + \sum_{i=1}^{N_u} w_i \left[1 - \frac{u_i(t_f)}{u_i^*} \right]^2 + w_{ext} \sum_{k=1}^{N_{ext}} \left[F_{ext,k}(t_f) \right]^2 \right\} \quad (27)$$

$\mathbf{b}$ is a vector containing slopes of trajectories of the external LN_2 streams; w_{ext} is the weight assigned to penalize the sum of squared deviations of LN_2 streams from zero at t_f. The variable $F_{ext,k}$ is the flow rate of the external LN_2 stream k. The external liquid can only be used to assisted transitions, and is required to be zero at the final steady state. This gives an additional set of constraints in the dynamic optimization

$$F_{ext,k}(t_f) \leq \varepsilon_{ext}, \quad k = 1, ..., N_{ext}. \quad (28)$$

Note that this design alteration requires modifications of tray material and energy balances with or without manual index reduction. For trays having external LN_2 entering, there would be an additional term in the balances. To illustrate, for a regular column tray having an external liquid nitrogen feed, $F_{ext,k}$, the material balance on component i at tray n becomes,

$$\frac{dm_{n,i}}{dt} = l_{n+1,i} + v_{n-1,i} - l_{n,i} - v_{n,i} + x_{\mathrm{LN}_2} F_{ext,k}.$$

The scenario selected is the 20 % demand increase case as the flooding constraint is active. In our study, this design modification was evaluated under base case impurity and tightened impurity requirements. Introduction of external LN_2 to the top multiple trays and single tray scenarios were compared. In this paper, we will present the optimization results for the multiple trays scenario.

We first consider the base case impurity path constraint limit of twice the steady-state limit,

$$Impurity_{path} = 2 \times Impurity_{ss}$$

Viewed another way, if the path constraint limit corresponds to the customer specification, then the steady-state impurity constraint limit includes a safety margin of 100 % to allow the customer specification limit to be adhered to both at steady-state operation and during transition. This set of studies conducted allowed the introduction of pre-stored LN_2 to the top three column trays. Dynamic optimizations were performed and the result compared against the scenario with no external liquid scenario (i.e., Section 5.2.1). Different combinations of control actions and control interval durations could result in similar dynamic performance, implying that when both duration times and slopes are allowed to change, there are too many degrees of freedom (DOF). As a result, the duration times of the control intervals were fixed at the optimal values obtained in the previous study to reduce the DOF in the problem and provide a clearer comparison between cases with and without external LN_2.

Optimization results are shown in in Fig. 6(a). With external LN_2 introduced, no significant improvement in the transition speed of the GN_2 production rate is observed. Optimal control profiles of the 4 basic manipulated variables in the two cases are also very similar. However, when the external liquid acts as additional reflux during transitions (i.e. non-zero flow rate at the solution), the product impurity peak is much lower during the transition. This observation suggests that a tighter impurity constraint can be imposed with the introduction of external reflux during transition, without sacrificing dynamic performance. We explore this next. Active constraints in this scenario are dew point and bubble point constraints at the PHX, and the flooding constraint in the column, as observed before.

We now consider the dynamic performance with additional reflux during transition under tightened impurity constraint limits. Case studies are conducted with the maximum impurity constraint level during transition reduced from twice to 1.2 times the steady-state impurity upper bound,

$$Impurity_{path} = 1.2 \times Impurity_{ss}.$$

This set of studies conducted allowed the introduction of pre-stored LN_2 to the top three column trays, and was solved following a similar approach as in the base case impurity level scenarios. The problem was solved first with four manipulated variables, including air feed, liquid air to the column, gas draw fraction and LN_2 production. Both trajectory slopes and control interval durations are optimized in the study. When external LN_2 was introduced, control durations times were fixed at the corresponding optimized durations obtained from the 4 MV case, and trajectory slopes were optimized.

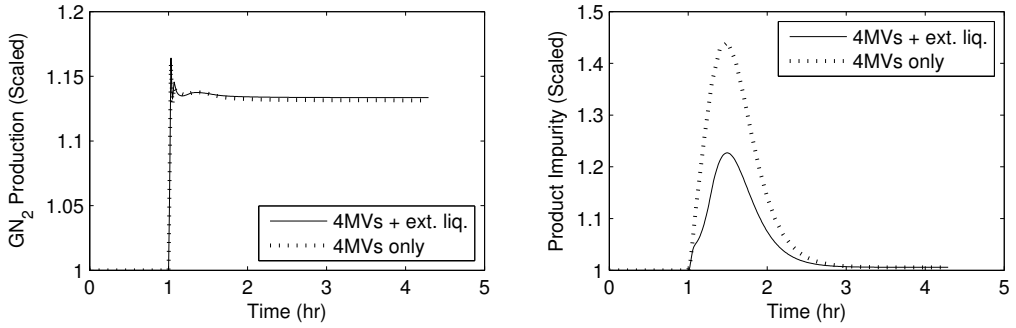

(a)

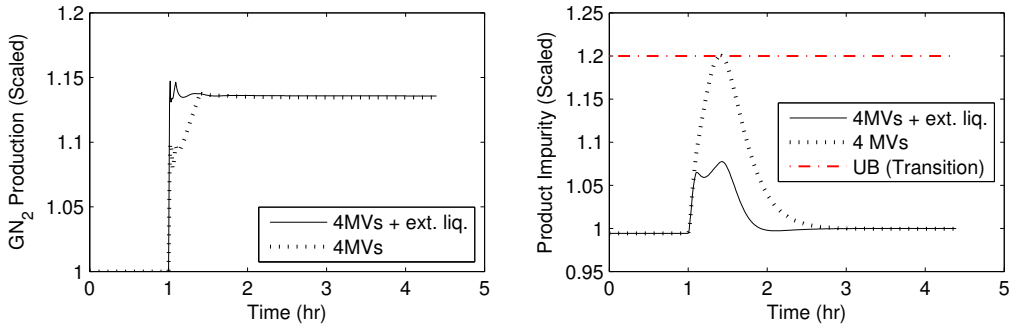

(b)

Figure 6: Optimized trajectories of scaled variables for 20 % demand increase cases with and without external liquid nitrogen with (a) base case impurity bound during transitions and (b) tightened impurity bound during transitions. Variables in the figure are scaled values.

Optimized trajectories are presented in Fig. 6(b). As shown, when the impurity constraint during transitions is tightened, when no external reflux is used, the speed of transition deteriorates, with the GN_2 production rate well below the desired value for a period of approximately 20 minutes. In this case, the impurity constraint is active during the transition. When external LN_2 is allowed, a significant increase in the transition speed can be achieved. The GN_2 production has a step-wise response as in the base case impurity cases (i.e., the GN_2 production almost immediately reaches and remains no lower than the desired value during the transition).

These studies demonstrate that introducing external LN_2 to the column during transition can improve the dynamic performance of the system. With this particular plant set-up and original impurity path constraint limit, introducing external LN_2 may not be very cost-effective as the improvement is not that significant. The system with four manipulated variables is seemingly capable of achieving acceptable dynamic performance without violating the flooding constraint during transition. However, when the impurity constraint during

transitions is tightened, significant reductions in transition speed (i.e., in terms of GN_2 production rate) can be achieved when external LN_2 is introduced. This suggests that when introducing external LN_2 is allowed, the plant does not require as large a safety margin to avoid violations of the customer purity specification during transitions. This in turn implies that the plant can operate with a higher maximum impurity level at steady state, leading to improved profitability.

5.3.2. Effect of Vent after the Compressor

We also investigated the effect of allowing a vent stream after the compressor for cases where the surge constraint may be active during transitions. Under normal conditions, the compressor operates on the right hand side of the surge line. Once the feed flow rate to the compressor reduces quickly below the restricted value, defined by the surge line (with fixed inlet guide vane angle in our case), a reversal of flow occurs as the compressor is incapable of working against the already-compressed gaseous stream downstream [40, 50]. Allowing a vent stream at the outlet of the compressor is the simplest form anti-surge control [50]. However, for this particular plant, allowing a vent stream may not be cost-effective as no significant improvement in transition speed was observed.

6. Conclusions

This study considered an optimization-based framework for improving the agility of a cryogenic N_2 plant in response to highly dynamic market conditions, specifically demand and electricity price fluctuations. Rigorous dynamic models for the plant were developed and served as a foundation for the later optimization studies. To investigate design limitations to transitions under varying product demand and electricity price, a two-tiered optimization formulation is proposed. First, a steady-state optimization problem is solved to determine the economically optimal steady-state operating point under a demand or electricity price change; thereafter, a dynamic optimization problem is solved to determine an optimal trajectory for rapid transition to the new operating point using a tracking based objective function. Use of manipulated variables as optimization degrees of freedom provides a limit of achievable performance, and also a benchmark for control performance analysis.

Through steady-state optimization, it was observed that under different demand and electricity price scenarios, it is optimal for the plant to operate with minimal LN_2 production,

and at the maximum allowable impurity level, except for demand decreases of 20% and 30% due to a restriction on the minimum air feed rate induced by a compressor surge constraint. Since the problem is non-convex, a number of optimization cases with differential initial guesses were solved and the best solution was reported as the optimal solution for each scenario.

The operating window of the plant is defined by the flooding constraint of the distillation column and the surge constraint of the compressor when the feed flow rate is considered. When the electricity price increases, before reaching a critical value, it is economically optimal to operate at high production levels; however, once the electricity price exceeds that value, it is beneficial to reduce production. We also considered these results from a different perspective, namely, providing demand response service to the grid, showing the importance of process *dynamics* when considering its operation as a demand response entity.

The optimal control trajectory obtained from solving dynamic optimization problems indicates the best achievable transition performance subject to plant constraints. The active constraints at the solution indicate design restrictions to more flexible and agile operation. Through analysis of the case study results, it was inferred that potential improvements in operation could be achieved through column tray, heat exchanger and compressor resizing/re-design.

In this paper, two design alternatives to improve the dynamic performance were investigated. Introducing external liquid to the column during transition with tightened impurity path constraint limits was shown to improve the dynamic performance of the system. This would allow a smaller safety margin for product purity, which would translate into more profitable steady-state operation. Allowing a vent stream after the compressor to prevent compressor surge does not result in a significant improvement in the dynamic performance for the plant configuration and operating conditions under consideration. However, a similar analysis applied to a different plant may lead to a different result and conclusions.

In this study, we did not consider the strategy of overproduction and storage of excess products an option due to the narrow time horizon, but we would like to explore this in our later studies. Future work involves extension to a multiproduct air separation plant, in which the problem dimension and complexity pose major challenges. Also under consideration is an optimal design formulation that captures economics, agility, disturbances and uncertainty such as ambient air temperature, model parameter uncertainty and demand and electricity price fluctuations. In a broader context, we will consider the interaction of production

scheduling and process control to fully realize the economic and grid-balancing benefits that can be derived from DR operation.

Acknowledgements

Support for this work from Praxair and the McMaster Advanced Control Consortium is gratefully acknowledged.

References

[1] M. J. Mohideen, J. D. Perkins, E. N. Pistikopoulos, Optimal design of dynamic systems under uncertainty, AIChE Journal 42 (1996) 2251 – 2272.

[2] C. A. Schweiger, C. A. Floudas, Interactions of design and control: Optimization with dynamic models, in: W. Hager, P. Pardalos (Eds.), Optimal Control: Theory, Algorithms, and Applications, Kluwer Academic Publishers, 1998, pp. 388 – 435.

[3] R. Baker, C. L. E. Swartz, Simultaneous solution strategies for inclusion of input saturation in the optimal design of dynamically operable plants, Optimization and Engineering 5 (1) (2004) 5 – 24.

[4] J. M. G. van Schijndel, E. N. Pistikopoulos, Towards the integration of process design, process control & process operability – current status & future trends, in: M. Malone, J. Trainham, B. Carnahan (Eds.), Foundations of computer aided process design 99, no. 323 in AIChE symposium series, American Institure of Chemical Engineers, 2000, pp. 99 – 112.

[5] V. Sakizlis, J. D. Perkins, E. N. Pistikopoulos, Recent advances in optimization-based simultaneous process and control design, Computers & Chemical Engineering 28 (10) (2004) 2069 – 2086.

[6] Z. Yuan, B. Chen, G. Sin, R. Gani, State-of-the-art and progress in the optimization-based simultaneous design and control for chemical processes, AIChE Journal 58 (6) (2012) 1640 – 1659.

[7] V. White, J. D. Perkins, D. M. Espie, Switchability analysis, Computers & Chemical Engineering 20 (4) (1996) 469 – 474.

[8] J. Miller, W. L. Luyben, P. Belanger, S. Blouin, L. Megan, Improving agility of cryogenic air separation plants, Industrial & Engineering Chemistry Research 47 (2008) 394 – 404.

[9] J. Miller, W. Luyben, S. Blouin, Economic incentive for intermittent operation of air separation plants with variable power costs, Industrial and Engineering Chemistry Research 47 (4) (2008) 1132–1139.

[10] R. Pattison, M. Baldea, Optimal design of air separation plants with variable electricity pricing, in: M. Eden, J. Siirola, G. Towler (Eds.), Proceedings of the 8th International Symposiun on Foundations of Computer Aided Process Design - FOCAPD, Elsevier, 2014, pp. 393–398.

[11] https://www.ferc.gov/industries/electric/indus-act/demand-response/dem-res-adv-metering.asp (2013).

[12] A. R. Sirdeshpande, M. G. Ierapetritou, M. J. Andrecovich, J. P. Naumovitz, Process synthesis optimization and flexibility evaluation of air separation cycles, AIChE Journal 51 (4) (2005) 1190 – 1200.

[13] Y. Zhu, S. Legg, C. D. Laird, Optimal design of cryogenic air separation columns under uncertainty, Computers & Chemical Engineering 34 (9) (2010) 1377 – 1384.

[14] Y. Zhu, S. Legg, C. D. Laird, A multiperiod nonlinear programming approach for operation of air separation plants with variable power pricing, AIChE Journal 57 (9) (2011) 2421 – 2430.

[15] S. Mitra, I. E. Grossmann, J. M. Pinto, N. Arora, Robust scheduling under time-sensitive electricity prices for continous power-intensive processes, in: FOCAPO 2012: Foundations of Computer-Aided Process Operations, Foundations of Computer-AidedProcess Operations, Savannah, Georgia January 8 - 11, 2012.

[16] M. Schenk, V. Sakizlis, J. D. Perkins, E. N. Pistikopoulos, Optimization-based methodologies for integrating design and control in cryogenic plants, in: J. Grievink, J. van Schijndel (Eds.), European Symposium on Computer Aided Process Engineering - 12, ESCAPE, Elsevier, The Hague, The Netherlands, 26 - 29 May, 2002, pp. 331 – 336.

[17] S. Bian, M. A. Henson, P. Belanger, L. Megan, Nonlinear state estimation and model predictive control of nitrogen purification columns, Industrial & Engineering Chemistry Research 44 (1) (2005) 153 – 167.

[18] R. Huang, V. M. Zavala, L. T. Biegler, Advanced step nonlinear model predictive control for air separation units, Journal of Process Control 19 (4) (2009) 678 – 685.

[19] Z. Xu, J. Zhao, X. Chen, Z. Shao, J. Qian, L. Zhu, Z. Zhou, H. Qin, Automatic load change system of cryogenic air separation process, Separation and Purification Technology 81 (3) (2011) 451 – 465.

[20] G. Zhu, M. A. Henson, L. Megan, Low-order dynamic modeling of cryogenic distillation columns based on nonlinear wave phenomenon, Separation and Purification Technology 24 (2001) 467 – 487.

[21] D. M. Espie, S. C. Papageorgaki, Validation of dynamic simulation models of cryogenic air separation processes, in: 11th Intersociety Symposium, Houston, Texas, USA, Houston, Texas, USA, January, 1998, pp. 91 – 98.

[22] Y. Cao, C. Swartz, M. Baldea, Design for dynamic performance: Application to an air separation unit, in: American Control Conference (ACC), 2011, IEEE, 2011, pp. 2683–2688.

[23] Y. Cao, Design for Dynamic Performance: Application to Air Separation Unit, Master's thesis, Department of Chemical Engineering, McMaster University, Hamilton (2011).

[24] B. Roffel, B. H. L. Betlem, J. A. F. Ruijter, First principles dynamic modeling and multivariable control of a cryogenic distillation process, Computers & Chemical Engineering 24 (2000) 111 – 123.

[25] V. Bansal, J. D. Perkins, E. N. Pistikopoulos, A case study in simultaneous design and control using rigorous, mixed-integer dynamic optimization models, Industrial & Engineering Chemistry Research 41 (4) (2002) 760 – 778.

[26] G. J. Prokopakis, W. D. Seider, Dynamic simulation of azeotropic distillation towers, AIChE Journal 29 (1983) 1017 – 1029.

[27] Y. S. Cho, B. Joseph, Reduced-order steady-state and dynamic models for separation processes. Part II. Application to nonlinear multi-component systems, AIChE Journal 29 (1983) 270 – 276.

[28] J. M. Smith, H. C. Van Ness, M. M. Abbott, Introduction to Chemical Engineering Thermodynamics, 7th Edition, McGRAW-HILL, 2005.

[29] V. Bansal, R. Ross, J. D. Perkins, E. N. Pistikopoulos, The interactions of design and control: Double-effect distillation, Journal of Process Control 10 (2000) 219 – 227.

[30] M. C. Georgiadis, M. Schenk, E. N. Pistikopoulos, R. Gani, The interaction of design, control and operability in reactive distillation systems, Computers & Chemical Engineering 26 (2002) 735 – 746.

[31] M. J. Lockett, Disitllation Tray Fundamentals, Cambridge University Press, 1986.

[32] D. W. Green, J. O. Maloney, R. H. Perry, Perry's Chemical Engineers' Handbook, McGRAW-HILL, 1997.

[33] R. C. Reid, J. M. Prausnitz, T. K. Sherwood, The Properties of Gases and Liquids, 3rd Edition, McGRAW-HILL, 1977.

[34] Infochem Computer Services Ltd, User Guide for Models and Physical Properties, Infochem Computer Services Ltd (2008).

[35] D.-Y. Peng, D. B. Robinson, A new two-constant equation of state, Industrial & Engineering Chemistry Fundamentals 15 (1) (1976) 59 – 64.

[36] A. U. Raghunathan, M. Soledad Diaz, L. T. Biegler, An MPEC formulation for dynamic optimization of distillation operations, Computers & Chemical Engineering 28 (10) (2004) 2037 – 2052.

[37] E. F. Costa Jr., R. C. Vieira, A. R. Secchi, E. C. Biscaia Jr., Dynamic simulation of high-index models of batch distillation processes, Latin American Applied Research 33 (2003) 155 – 160.

[38] M. Fikar, M. A. Latifi, Y. Creff, Optimal changeover profiles for a industrial depropanizer, Chemical Engineering Science 54 (1999) 2715 – 2720.

[39] D. Ballard, C. Brosilow, C. Kahn, Dynamic simulation of multicomponent distillation columns, in: AIChE Meeting, Paper No. 42a, Miami, Miami, USA, October, 1978.

[40] R. N. Brown, Compressors: Selection and Sizing, ELSEVIER, 2005.

[41] Process System Enterprise Ltd, gPROMS v 3.3.1, http://www.psenterprise.com/ (2010).

[42] Process System Enterprise Ltd, Optimisation and Model Validation with gPROMS (2009).

[43] V. S. Vassiliadis, R. W. H. Sargent, C. C. Pantelides, Solution of a class of multistage dynamic optimization problems. 2. problems with path constraints, Industrial & Engineering Chemistry Research 33 (9) (1994) 2123 – 2133.

[44] Process System Enterprise Ltd, Personal Communication (2010).

[45] D. Todd, M. Caufield, B. Helms, M. Starke, B. Kirby, J. Kueck, Providing reliability services through demand response: A preliminary evaluation of the demand response capabilities of Alcoa Inc, Oak Ridge National Laboratory Technical Report ORNL/TM-2008/233 (2008).

[46] M. Paulus, F. Borggrefe, The potential of demand-side management in energy-intensive industries for electricity markets in germany, Applied Energy 88 (2) (2011) 432–441.

[47] Y. Zhu, S. Legg, C. Laird, Optimal operation of cryogenic air separation systems with demand uncertainty and contractual obligations, Chemical Engineering Science 66 (5) (2011) 953–963.

[48] S. Mitra, J. Pinto, I. Grossmann, Optimal multi-scale capacity planning for power-intensive continuous processes under time-sensitive electricity prices and demand uncertainty. Part I: Modeling, Computers & Chemical Engineering 65 (2014) 89 – 101.

[49] M. Baldea, I. Harjunkoski, Integrated production scheduling and process control: A systematic review, Computers and Chemical Engineering 71 (2014) 377–390.

[50] R. F. Neerken, Keys to compressor selection, in: R. Greene (Ed.), The Chemical Engineering Guide to Compressors, McGRAW-HILL, 1984, pp. 14 – 30.